NASA Precipitation Measurements Missions (PMM) Science Team Meeting, Denver, CO, 7 – 11 November, 2011

Application of AMSR-E and a Ground-based Radar to Assess Cloud Microphysical Schemes in the WRF Model for a Winter Storm

Mei Han[1,2], Scott A. Braun[2], Toshihisa Matsui[3,2], Christopher R. Williams[4,5]

[1]Goddard Earth Sciences Technology and Research (GESTAR), Morgan State University; [2]Laboratory for Atmospheres, NASA/GSFC;
[3]University of Maryland, [4]Cooperative Institute for Research in Environmental Sciences, University of Colorado; [5]NOAA/Earth System Research Laboratory

I. INTRODUCTION

On December 30-31, 2005, a landfalling winter cyclone caused intense precipitation in the California and Nevada mountain and valley regions with a high hydrological impact. It was sampled by NASA satellites, TRMM and Aqua, and a wide variety of ground-based instruments deployed by the NOAA Hydrometeorological Testbed (HMT) program. In this study, we apply the Advanced Microwave Scanning Radiometer – Earth Observing System (AMSR-E) and a ground-based S-band precipitation profiling radar (S-prof), as well as simulations from the Weather Research and Forecasting (WRF) model to investigate the precipitation system. Simulated brightness temperature, radar reflectivities and doppler velocities are validated with the observations. Sensitivity of different microphysical schemes on precipitation structure and their influences on brightness temperature, reflectivity and doppler velocity calculations are examined.

II. BACKGROUND OVERVIEW

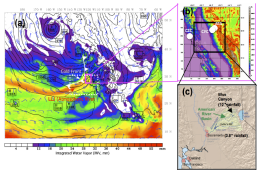

Fig. 1 (left): (a) Synoptic view of Integrated water vapor (shaded, mm), SLP (contoured, hPa), and surface winds, (b) Terrain height in California, and (c) American River Basin. White dots indicate locations of S-prof sites.

- Intense baroclinic zones between polar and subtropical air masses.
- Prefrontal low-level jets (LLJ) in the cyclone's warm sector transport abundant moisture onshore (often called an "atmospheric river")
- Highly complex terrain in California (CA)
- Significant orographic precipitation enhancement in the American River Basin

III. OBSERVATIONS: AMSR-E

The Brightness Temperature (Tb) at AMSR-E high frequency channels, 89 GHz, and the Polarization-Corrected Temperature (PCT) are examined. PCT89 = 1.82Tb89v – 0.82Tb89h, which is useful to differentiate low-emissivity water bodies from scattering due to precipitation ice. .

- Tb shows a plume of strong water vapor flux (the atmospheric river) reaching the CA coastal region
- Tb depression indicates scattering by precipitation ice and/or large raindrops near coastal region and over Sierra Nevada range
- PCT (c and d) show distinct scattering signature of the precipitation system

Fig. 2: AMSR-E 89 GHz Tb and PTC at 10:16 UTC 31 Dec 2005

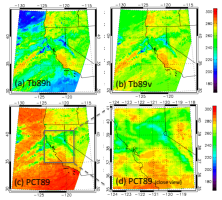

IV. OBSERVATIONS: S-PROF

During this event, S-band precipitation profiling radars (S-prof) were deployed at Alta (ATA, 1085 m MSL) and Colfax Water (CFC, 636 m MSL) over Sierra Nevada, and Cazadero (CZC, 475 m MSL) over coastal ranges by NOAA's HMT program, see Fig. 1b for locations of the S-prof sites.

Fig. 3: S-prof observations on 31 December 2005.

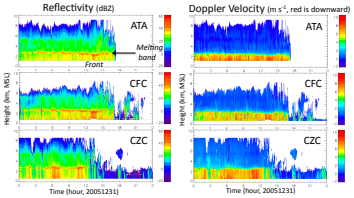

Fig. 4: Histogram

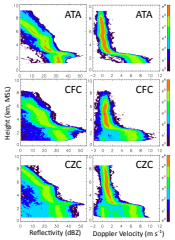

- Wide-spread moderate precip. and periods of intense precip. associated with the frontal passage toward the end of the event.
- Evident bright band (@ ~3km MSL) and secondary reflectivity maximum (@ ~5-6 km MSL).
- Reflectivity magnitude: Rain layer: 25 – 45 dBZ; Snow layer: < 30 dBZ
- Doppler velocity magnitude: Rain layer: 5 – 10 m s^{-1}; Snow layer: < 2 – 3 m s^{-1}

V. WRF SIMULATIONS

High resolution WRF simulation (1.3 km horizontal spacing) is used to further investigate the precipitation structure. Simulations with four different microphysical schemes, Goddard (GSFC), WSM6, Thompson (THOM), and Morrison (MORR), are investigated. See Table 1 (below) for some details about particle size distribution (PSD) assumptions etc.

All the hydrometeor species in these schemes adopt a gamma function:

$$N(D) = N_0 D^{\mu} e^{-\lambda D}$$

with the shape factor equal to zero (or exponential function) and are assumed as sphere shapes, except snow in THOM scheme. The latter uses a PSD assumption following Field et al. (2005) with a m-D relationship of $m = 0.069 D^2$.

Table 1: PSD assumptions for 4 schemes

	# of moment	PSD (μ= 0?)			Fixed or Varied N_0 (m^{-4})?			M-D (if sphere?)			Bulk density ρ_x (kg/m^3)		
		Sn	Gr	Ra	Sn	Gr	Ra	Sn	Gr	Ra	Sn	Gr	Ra
WSM6	1	0	0	0	N_{0r} (T)	4.e6	8.e6	y	y	y	100.	500.	1000.
GSFC	1	0	0	0	3.6e7	4.e6	8.e6	y	y	y	100.	400.	1000.
THOM	1.5	NA	0	0	effective N_{0r} (Tx)	N_{0r} (Ux)	N_{0r} (Ux)	n	y	y	not a const.	400.	1000.
MORR	2	0	0	0	N_{0r} (Ux)	N_{0r} (Ux)	N_{0r} (Ux)	y	y	y	100.	400.	997.

Fig. 5 (right): Mean profiles of different hydrometeor species at 10 UTC 31 Dec. 2005.

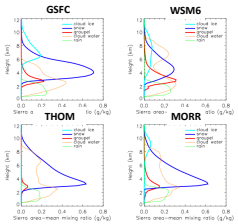

- GSFC: more snow, shallower cloud liq.
- WSM6: least snow, most graupel
- THOM: least cloud ice, least graupel
- MORR: similar snow and cloud liq. to THOM, moderate amount of graupel

VI. SIMULATED PCTs

The WRF outputs are ingested into the Goddard Satellite Data Simulation Unit (SDSU) to calculate the brightness temperature at 89 GHz. PCT89 is evaluated. To further investigate the contribution from snow vs. graupel, partitioned PCT89 is also calculated.

- Simulated PCT89 are lower by 20 K or more than the observed values, indicating the simulated scattering was too strong.
- Snow contributes most to the large amount of scattering in the GSFC and MORR runs due to their dominant mass of snow.
- Graupel is a big contributor to scattering in the WSM6 run.
- Graupel generally has a larger contribution to scattering than snow when their water paths are comparable.

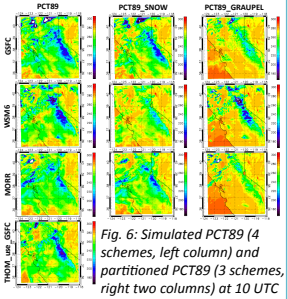

Fig. 6: Simulated PCT89 (4 schemes, left column) and partitioned PCT89 (3 schemes, right two columns) at 10 UTC 31 Dec. 2005.

VII. SIMULATED REFLECTIVITY

Customized reflectivity is calculated for each simulation with different microphysics scheme.

For spheres, $Z_e \propto \int_{D_{min}}^{D_{max}} D^6 N(D) dD$; For snow in THOM (non-spheres), $Z_e \propto \int_{D_{min}}^{D_{max}} m(D)^2 N(D) dD$

Fig. 7: Simulated reflectivity on 31 December 2005

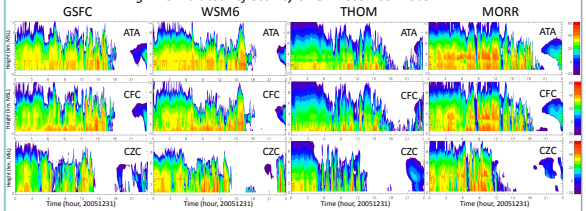

Fig. 8: Histogram for simulated reflectivity

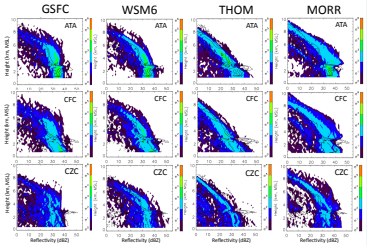

- Melting band is not captured in simulations
- Different precipitation structure shown along with frontal passage
- Reflectivity magnitudes:
  1) GSFC and WSM6 appears similar: agree to Obs. well in the rain layer, too strong reflectivity in the snow layer
  2) THOM agrees well with Obs.
  3) MORR are too strong, in rain and snow layers.

To understand why the simulated reflectivity have large differences among these schemes, we calculated the effective radius for snow. Effective radius is defined as:

$$r_e = \frac{\int N(D) D^3 dD}{\int N(D) D^2 dD}$$, following McFarquhar and Heymsfield, 1996.

Fig. 9 (right): Histogram of snow effective radius at 10 UTC 30 Dec. 2005.

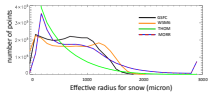

- GSFC, WSM6 and MORR have more larger snow particles
- MORR has more particles larger than 2 mm
- THOM has more small particles

VIII. SIMULATED DOPPLER VELOCITY

Doppler velocity is simulated for GSFC, WSM6, and MORR schemes at the S-prof sites. The doppler velocity (dopvel) is the sum of hydrometeor's terminal velocity and vertical air motion for the vertical pointing radar. The total terminal velocity is reflectivity-weighted:

$$Vt = Vt_{s+g+r} = \frac{\int N_s \sigma_s(D) V_s(D) dD + \int N_g \sigma_g(D) V_g(D) dD + \int N_r \sigma_r(D) V_r(D) dD}{\int N_s \sigma_s(D) dD + \int N_g \sigma_g(D) dD + \int N_r \sigma_r(D) dD}$$

, where $V_x = a_x D^{b_x} (\frac{\rho_0}{\rho})^c$ is the particle fall velocity. See Fig. 10 (right) for the relationship of V and D for rain (crosses), graupel (triangles), snow (stars) particles.

Fig. 10: Particle fall velocity

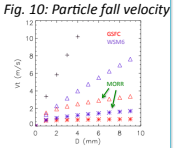

Fig. 11 (right): Simulated doppler velocity on 31 Dec 2005

Fig. 12 (below): Histogram for simulated doppler velocity

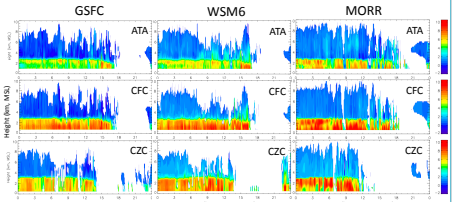

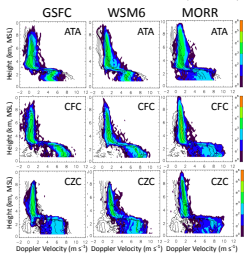

- WSM6 and MORR have faster dopvel than GSFC in snow layer
- GSFC dopvel is comparable to Obs. in snow layer
- Simulated dopvel in rain layer vary with respect to locations
  1) ATA: both GSFC and WSM6 are slower than Obs. MORR agrees with Obs. better
  2) CFC: all schemes are faster than Obs.
  3) CZC: schemes appear closer to Obs.

VIIII. SUMMARY AND FUTURE WORK

Observations from passive and active microwave sensors onboard satellite or ground-based are used to study a heavy precipitation system associated with a landfalling winter cyclone in the US West Coastal region. The structure and evolution of the system were well captured by the high frequency channels of AMSR-E and an S-band precipitation profiling (S-prof) radar. WRF simulations with 4 different microphysics schemes show discrepancies in the vertical profiles of hydrometeor species. Customized simulations of brightness temperature, reflectivity and doppler velocity have been developed for these schemes. Analysis of simulated brightness temperatures show that the simulated scattering is considerably stronger than the observations, possibly due to a large amount of snow and/or graupel. The major contributor to scattering is snow in the GSFC and MORR runs, while it is graupel in the WSM6 run. The simulated reflectivity and doppler velocity are evaluated with the radar observations. Reflectivity simulated with GSFC, WSM6, and MORR schemes are stronger than the observations, particularly in the snow layer. THOM scheme show a better agreement to the observed reflectivity. Simulated doppler velocity generally agrees with the observations. GSFC has a better agreement than WSM6 and MORR in the snow layer. Performance of model simulating doppler velocity in the rain layer varies with respect to the location of the sites. Future work will focus on in-depth understanding of how the differences in microphysical schemes lead to the discrepancies of brightness temperature, reflectivity and doppler velocity simulations.